Complex geometries in additive manufacturing: A new solution for lattice structure modeling and monitoring

Bianca Maria Colosimo, Marco Grasso, Federica Garghetti, and Beatrice Rossi

Complex geometries in Additive Manufacturing: a new solution for lattice structure modelling and monitoring

Colosimo, B.M., Gaghetti, F., Grasso, M.

Politecnico di Milano, Dipartimento di Meccanica, Politecnico di Milano

Via La Masa 1, 20156, Milano, Italy

Abstract. The production of novel types of complex shapes is nowadays enabled by new manufacturing paradigms such as additive manufacturing. The continuous increase of shape complexity imposes new challenges in terms of inspection, product qualification and process monitoring methodologies. Previously proposed methods for 2.5D free-form surfaces are no longer applicable in the presence of this kind of new full 3D geometries. This paper aims to tackle this challenge by presenting a statistical quality monitoring approach for structures that cannot be described in terms of parametric models. The goal consists of identifying out-of-control geometrical distortions by analysing either local variations within the part or changes from part to part. The proposed approach involves an innovative solution for modelling the deviation between the nominal geometry (the originating 3D model) and the real geometry (measured via x-ray computed tomography) by slicing the shapes and estimating the deviation slice by slice. 3D deviation maps are then transformed into 1D deviation profiles enabling the use of a profile monitoring scheme for local defect detection. The feasibility and potential of this method are demonstrated by focusing on a category of complex shapes where an elemental geometry regularly repeats in space. These shapes are known as *lattice structures*, or *metamaterials*, and their trabecular shape is thought to provide innovative mechanical and functional performance. The performance of the proposed method is shown in real and simulated case studies.

Keywords: complex shape; lattice structure; statistical quality monitoring; profile monitoring; additive manufacturing; 3D printing.

1. Introduction

Thanks to the advent of new manufacturing and inspection technologies, a novel class of complex shapes is going to spread. Since the first seminal developments in statistical quality monitoring

applications, the analysis of dimensional and geometrical features has evolved from univariate to multivariate quality characteristics, and then from profile data to surface measurements and high dimensional point clouds. Fig. 1 depicts this evolution, driven by continuous technological developments in industry. Nowadays, the shape complexity of products is no longer limited to simple 2.5D free-form surfaces, as completely new levels of design freedom have been made available. The increased capability of producing these brand new 3D geometries is imposing the need to rethink and innovate the statistical quality monitoring methodologies adopted in discrete manufacturing processes.

$X = D \in \mathbb{R}$ — Univariate quality characteristic

$\mathbf{X}=[D,L,OOC,...]'$ $\mathbf{X} \in \mathbb{R}^p$ — Multivariate quality characteristcs

$X = f(\theta) + \varepsilon$ — Profile data

$X = f(\theta,z) + \varepsilon$ — Surface data and point-clouds

? — Novel complex shapes
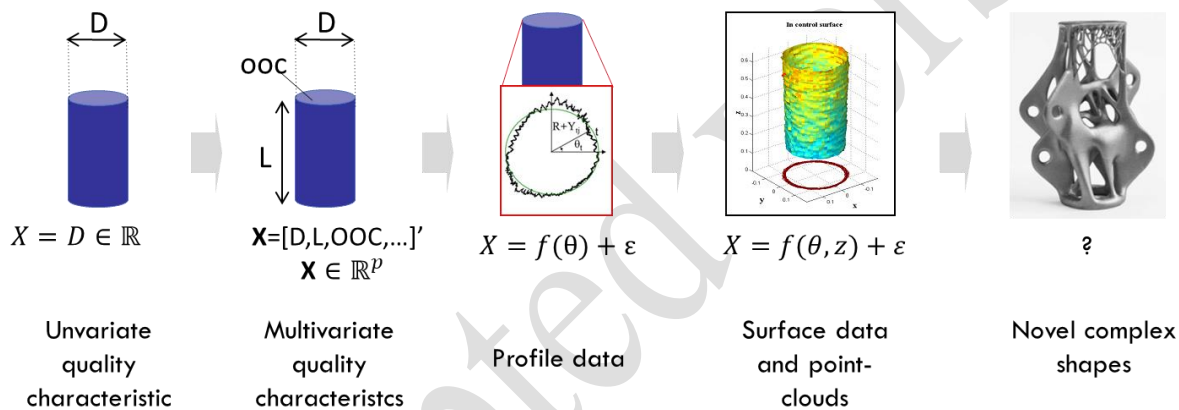
Fig. 1 – Example of the evolution of shape complexity in industrial statistical quality monitoring problems (the picture of the complex shape on the right is from Galjaard et al., 2014)

The proposed approach belongs to the family of statistical quality monitoring approaches for complex shapes that involves the analysis of a map showing the deviation of the manufactured shape from the nominal shape, i.e., the originating Computer Aided Design (CAD) file. Analysis of deviations also represents the basic approach as far as quality inspection is concerned, i.e., to decide whether the deviation map observed is compatible with the specifications. However, compared to existing literature (see also the review in Section 2), the proposed approach presents a first novel contribution in the way in which the deviation map is modelled and monitored. In fact, most of the existing

approaches for quality monitoring of complex shapes and surfaces entail an extension of the profile monitoring methodology (Colosimo et al., 2014; Del Castillo et al., 2015; Wang et al., 2014; Zang and Qiu, 2018a, 2018b). At a first stage, a model is created to represent the deviation observed at each location, e.g., in case of Cartesian coordinates, $d(x, y, z) = f(x, y, z) + e(x, y, z)$, where the term $f(\cdot)$ represents a large-scale parametric model and the term $e(\cdot)$ represents the noise term, which can be iid or have a spatial autocorrelation structure to be modelled as well. Then, the model is fitted to each surface and the coefficients are included in one vector that is monitored by means of multivariate control charting schemes, whereas a second control chart can be used to monitor the residual noise variance. Starting from this seminal idea, various other solutions have been proposed, including nonparametric methods or Gaussian processes for modelling the deviation map: the control chart is built on the vector of deviations between the fitted model and the measured data at a given set of checkpoints defined as a reference (Colosimo et al., 2014; Del Castillo et al. 2015, Wang et al., 2014, Zang and Qiu, 2018a and 2018b).

Passing from free-form surfaces to full 3D shapes, methods based on surface modelling and/or point-to-point discrepancy analysis become computationally expensive or even intractable. We propose a method with a first novelty aspect that regards the shift from point-to-point deviations to deviations modelled at "sub-unit" or "sub-feature" level. The underlying idea consists of dividing the complex shape into sub-features and estimating their local deviation maps. In the proposed approach, each deviation map is modelled by *slicing* the shape and looking at the deviation from the nominal geometry in each slice, as it is usually done for image and video-image data. Thanks to this slicing operation, it is possible to transform a complex 3D deviation map into a set of 1D deviation *profiles*, one for each sub-feature, which associates one estimated deviation value to each slice. This approach allows one to easily apply profile monitoring methods to very complex 3D point clouds, by capturing spatial patterns of local deviations as well, along one predefined direction, i.e., the direction along which the slicing was applied.

The proposed approach also provides a novel perspective compared to other studies that proposed

summarizing the quality information enclosed in 3D point clouds. In previous literature, the deviation map was summarized as a whole, using a quantile-quantile (Q-Q) plot (Megahed et al., 2010; Wells et al., 2013) or by considering a set of average deviations in different regions of interest (Huang et al., 2018; Stankus and Castillo-Villar, 2018). Representing the deviation in the form of a Q-Q plot yields the loss of any information about the spatial dependence of the deviations and, being a global approach, it prevents comparing deviation patterns in different locations of the part. On the other hand, computing an average deviation in different regions of the shape enhances the detection of local anomalies, but the use of average deviations may filter out potential "signatures" of interest in the deviation pattern.

As an important by-product, the proposed solution has a direct connection with additively manufactured (or 3D printed) parts, as they are produced according to a layer-wise (i.e., slice by slice) paradigm. In this framework, by combining the slicing operation with the profile monitoring scheme, it is possible to be consistent with the natural way in which the part is built.

A second main contribution of this study regards the quality problem addressed, which entails complex 3D geometries that go beyond 2D and 2.5D surface data usually investigated in mainstream literature. In particular, this study addressed a novel class of quality problems, where an elemental geometry regularly repeats within the structure, i.e., any cellular structure with non-stochastic geometry of the cell. In this framework, the paper specifically focuses on a category of complex shapes that has been gaining increasing interest in industry, known as *lattice structures* (Wu et al., 2019). In lattice structures, the elemental geometry that regularly repeats in space is usually characterized by a trabecular cell (Fig. 2a). These structures also belong to the category of *metamaterials*, as they gain their functional properties from their structure rather than inheriting them directly from the material they are composed of (Wu et al., 2019).

The industrial interest in lattice structures is due to the many interesting properties that make them an effective solution in a wide range of applications (Fig. 2b, c, d). They combine a lightweight design with high specific stiffness and strength, resulting in high stiffness-to-weight ratios required in the

aerospace and racing sector (Fig. 2c, d). Their regular structure also yields isotropic performance that make them preferable to more consolidated lightweight designs. They enable many more additional benefits, e.g., enhanced osteo-integration and compatibility with the human tissues for bio-medical applications (Fig. 2b), advanced heat exchanging properties, and high energy absorption capabilities.
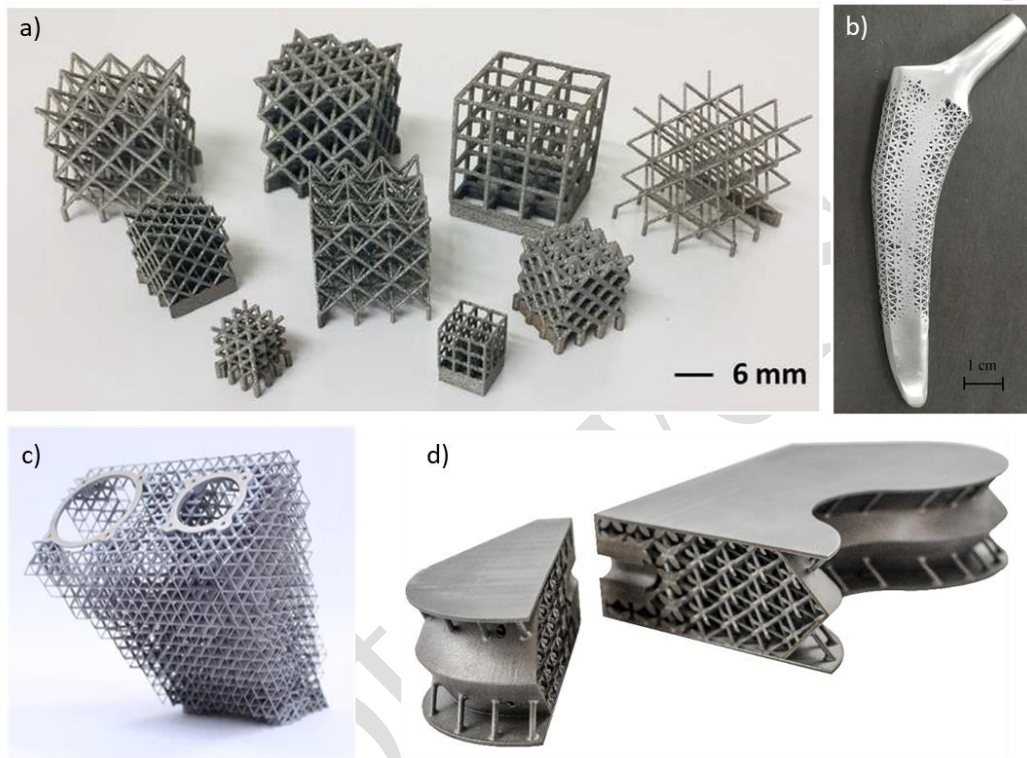
Fig. 2 – Examples of lattice structure geometries (a) (Hanks et al, 2020) and examples of their industrial applications: b) hip implant (Wang et al. 2018), c) support bracket for space application (Komarek et al., 2017), d) titanium insert for aerospace applications[1]

Since lattice structures involve unit cell geometries that regularly repeat in space, it is particularly critical to define and develop new methods that allow one to determine the variability of the geometrical properties within the part and from part to part.

Starting from a geometrical reconstruction of the lattice structure via x-ray computed tomography (CT), the spatial map of deviations from the nominal geometry is sliced and modelled in the form of

---

[1] https://commons.wikimedia.org/wiki/File:Atos_titanium_insert_Courtesy_of_Materialise.jpg

deviation profiles associated with each individual unit cell. The pattern of the deviation profile is representative of the natural signature of the process that, in the absence of special causes, should repeat from cell to cell.

The performance of the proposed approach is demonstrated by means of both simulated and real data involving metal lattice structures manufactured via laser powder bed fusion. The method is compared against a benchmark approach representative of a simple industrial practice, which relies on monitoring a synthetic quality index commonly used in literature devoted to lattice structure characterization (Van Bael et al., 2011).

The study focuses on industrial metal AM applications involving qualification procedures requiring homogeneous design and process conditions throughout production. Nevertheless, the proposed approach is open to possible use in one-of-a-kind applications too. Indeed, by characterizing the deviation profile of each unit cell within the part it could be possible to detect outlying cells characterized by an anomalous pattern compared to other cells. This potentially allows one to identify local weaknesses in the structure even if the overall shape of the component changes from build to build. Therefore, the proposed approach is suitable for monitoring the stability of the production process over time, but also for detecting local geometrical distortions in one single part, making it possible to develop conformity criteria.

Moreover, although the proposed method is presented for application to lattice structures, it can be easily applied to any other complex shape, as the slicing operation is applicable to any geometry. This allows practitioners to rely on the extensive literature on profile monitoring to complete the quality-monitoring task.

The paper is organized as follows. Starting from a state-of-the-art overview of statistical quality monitoring methods for complex shapes in Section 2, a motivating case study is presented in Section 3 and the proposed approach is then described in Section 4. Section 5 presents a simulation analysis aimed at assessing the performance of the proposed approach and highlighting its enhanced performance compared to a benchmark competitor. Section 6 presents further results based on a real

case study to demonstrate the practical use of the method. Section 7 concludes the paper.

2. Statistical quality monitoring of complex shapes

The continuously enhanced capability to produce complex shapes in discrete part manufacturing has motivated increasing research in the field of statistical analysis and statistical quality monitoring of complex geometries and spatially dense metrology data.

Mainstream literature focuses on the analysis of free-form surfaces based on 2.5D or 3D point-cloud data for different kinds of applications, from inspection to process monitoring and reverse engineering. The capability to model 2.5D surfaces enabled the extension of statistical quality monitoring methods from profile data to surface measurements and high-dimensional point-clouds. Relying on this, one major stream of research involves the use of model-based approaches, where a spatial model was fitted to the measured deviation from a nominal surface and combined with a multivariate statistical quality monitoring technique (Colosimo et al., 2014; Wang et al., 2014; Zang and Qiu, 2018a, 2018b).

Colosimo et al. (2014) presented an extension of statistical process monitoring methods from profile to surface data, where a Gaussian Process (GP) was used as a tool for surface monitoring as it simplifies the modelling step by avoiding the need to select appropriate regressors. Based on the GP-fitted surface, a control charting scheme was proposed for monitoring the deviations from the in-control pattern estimated in phase I in correspondence to predefined checkpoints.

Relying on a Gaussian-Kriging model, Wang et al., (2014) presented a surface monitoring approach applied to the vector of surface model parameters representing quality characteristics of interest. Del Castillo et al. (2015) showed that a geodesic GP, which considers correlations between two points on the surface as a function of their geodesic distance on the surface, enables a better free-form surface reconstruction than that obtained by relying on Euclidean distances. A nonparametric kernel smoothing method for surface data was proposed by Zang and Qiu (2018a and 2018b). In phase I,

Zang and Qiu (2018a) proposed monitoring the maximum deviation from an in-control surface model, whereas, in phase II Zang and Qiu (2018b) proposed a CUSUM monitoring scheme for the absolute deviations.

Other authors proposed methods for the analysis of deviation maps using summary statistics or models in lower dimensional spaces. In this stream of research, some authors (Megahed et al., 2010; Wells et al., 2013) proposed synthetising the information enclosed by the 3D deviation map in terms of the quantile-quantile (Q-Q) plot of the distribution of point deviations from the nominal shape. A profile monitoring approach was then applied to monitor the Q-Q curve. This method allows one to represent the whole deviation in the form of a 1D curve, with the possible loss of local information. Other authors proposed dividing the deviation map into regions of interest (ROIs) and estimate synthetic descriptors in each ROI. Stankus and Castillo-Villar (2018) combined this method with a multivariate generalized likelihood ratio (GLR) control chart to monitor the mean deviation in each ROI. Similarly, Hiang et al. (2018) proposed a statistical monitoring method where small sub-regions of a complex shape were characterized by two synthetic indexes, namely the non-random distribution of abnormal points and the plane direction deviation of a sub-region. He et al. (2017) proposed a 2D version of this approach, by first projecting the original 3D deviation map onto a 2D space in one predefined direction. ROI-based methods allow one to detect and analyse local anomalies but estimating the synthetic descriptors may filter out some relevant process "signatures".

A different research stream deals with some recent studies on statistical quality monitoring methods for manifold data. In this field, rather than fitting a spatial model to the surface, Zhao and Del Castillo (2019) and Del Castillo and Zhao (2019) proposed a statistical quality monitoring approach based on monitoring "intrinsic" quantities of the surface that are invariant to rigid transformations and do not depend on distances across the 3D Euclidean space in which the part exists. Shi et al. (2019) focused on identifying the nature of part-to-part variations in the presence of manifold data without any prior knowledge of the variation patterns.

In addition, it is worth mentioning that other methods, despite being proposed for image data, may

potentially be suitable for or adapted to complex shapes. As an example, Menafoglio et al. (2018) presented a study where a destructive inspection of random cellular structures led to image-based quality monitoring. The probability density function (PDF) of a synthetic descriptor computed in each image was used to detect out-of-control changes of cell morphology. Similarly, Bui and Apley (2018) proposed a method for detecting changes in the nature of stochastic textures by monitoring the joint distribution of pixel intensities, assuming that 2D image data was characterized by random patterns, without any golden standard.

As mentioned in the introduction, the proposed approach belongs to the family of methods that entail estimating a deviation map between the manufactured shape and a nominal prototype. Compared to the aforementioned literature, the proposed method entails a different perspective on the way in which the deviation map can be modelled and monitored, opening up to statistical quality monitoring of 3D shapes and structures the complexity of which goes beyond that of 2D and 2.5D surfaces.

3. The lattice structure case study

Lattice structures with regularly repeating unit cells represent the complex shapes that motivate the present study. These structures are well suited to being produced using additive manufacturing but there is still a lack of statistical quality monitoring tools in industry (Colosimo, 2018). Detecting local defects in these complicated geometries is highly relevant, as outlined by various authors (Liu et al., 2017; Melancon et al., 2017; Dallago et al., 2019). Indeed, local geometrical and dimensional inaccuracies of the unit cells may have a detrimental effect on the elastic modulus and compressive strength of the structure. As an example, Liu et al. (2017) showed that the magnitude of strut oversizing/undersizing influences the type of failure mechanism, whereas Melancon et al. (2017) pointed out that a geometrical mismatch between the produced specimen and the originating CAD model may affect osteo-integration performance in biomedical applications.

In the following sections of this paper, the term "as-built geometry" is used to indicate the geometry of the produced lattice structure reconstructed by means of non-destructive inspections, and the term

"as-designed geometry" to indicate the original CAD model used to produce the structure.

The case study considered in this paper consists of a lattice structure with a designed porosity of 90%, which provides a very high stiffness-to-weight ratio and, at the same time, advanced energy absorption performance. The lattice structure consists of $N = 64$ dodecahedron unit cells of size $l = 10\ mm$ within a specimen of dimension $40\ \times\ 40\ \times\ 40$ mm. Each unit cell consists of 32 prismatic elements with a strut diameter of 0.67 mm. Fig. 3a shows top, side and 3D views of the dodecahedron unit cell.

The lattice structure was produced by Laser Powder Bed Fusion (LPBF) of A357 Al-Si-Mg aluminium alloy with a particle size in the range $20 - 63$ μm. Two copies of a cubic lattice specimen, hereafter denoted as specimen A and specimen B, were produced using a Renishaw AM250 system with the process parameters shown in Table 1. The specimens were produced with two $40\ \times\ 40$ mm thin walls of 0.6 mm wide, on opposite sides of the structure to enable additional measurements and tests not considered in this study. The geometrical accuracy analysis was limited to the lattice structure that separates the thin walls.

The specimens' location within the build area and a sample image of specimen A is shown in Fig. 3b.
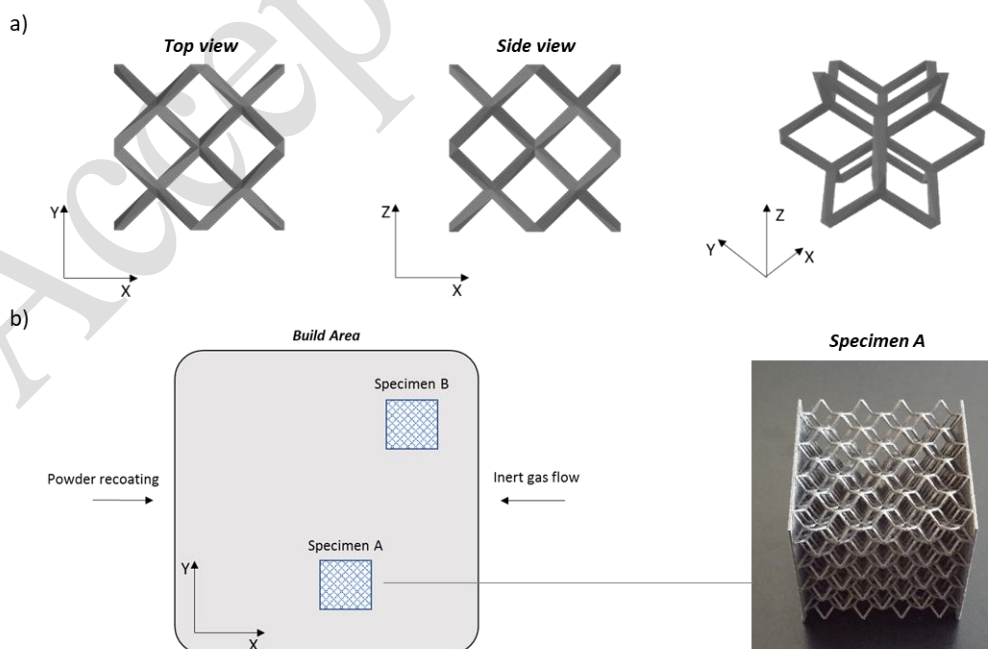
Fig. 3 – a) Top view (left), side view (right) and 3D view of the dodecahedron unit cell; b) Specimen location within the build area (left) and example of as-built specimen (right)

Table 1 – LPBF process parameters

Scan strategy	Scan mode	Laser power	Exposure time	Point distance	Hatch distance	Layer thickness
Meandering	Pulsed	200 W	140 μs	80 μm	130 μm	25 μm

The as-built specimens were inspected using a North Star Imaging X25 X-ray CT scan system with a resolution or 33 μm. Fig. 4 shows some examples of slice images generated by the x-ray CT scan of the as-built lattice specimen A. Each slice includes 4 × 4 unit cells.
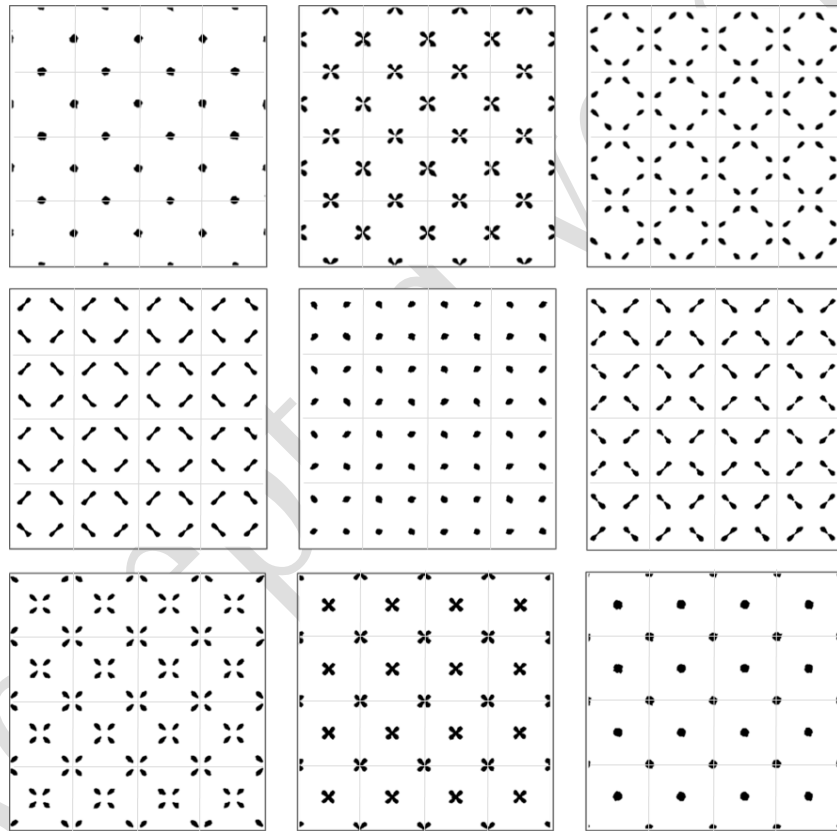
Fig. 4 – Example of images obtained by slicing the as-built 3D mesh of the lattice structure (vertical and horizontal grey lines are superimposed onto the as-built slices to show the partition into 4 × 4 unit cells)

In order to introduce on purpose a variation between the geometrical and dimensional properties of the two specimens, an anomaly of the inert gas flow was used as defect driver. In particular, a non uniform gas flow was generated in the location of the build area where specimen B was placed (see Fig. 3b). The effect of this anomaly was investigated in a previous study by using the same gas flow

settings on the same machine, the same process parameters and the same A357 aluminium powder (He et al., 2019). It is known that a non-uniform gas flow may produce a lower dimensional accuracy of the final part. Since this is an undesired source of variability with an assignable cause, it is worth signalling the resulting effect on the monitored parts.

The dataset can be made available by the authors upon request.

4. Proposed methodology

The overall method relies on three major assumptions: i) The possibility of representing the monitored structure as the union of unit cells of fixed geometry that regularly repeats in space. ii) The application in a production framework, where all process parameters are kept fixed. iii) The use of post-process (ex-situ) x-ray CT for shape reconstruction. X-ray CT is a standard for many mission-critical and high-value-added components in industry, and it represents the only way to reconstruct both external and internal features.

Assumption i) applies to a wide range of industrial products where enhanced functional performance is achieved thanks to lattice structures. Extensions of the proposed approach or alternative solutions could be considered when dealing with structures in which the unit cell's morphology varies within the part, such as in products in which the lattice shape adapts to the manifold it belongs to.

The rationale behind assumption ii) is that industrial qualification procedures in metal AM currently require that both design parameters and process parameters are kept fixed, in agreement with the ISO/ASTM standards in AM. In particular, the ISO/ASTM 52904 standard (ISO/ASTM, 2019) specifies that, once the machine has been calibrated, all the machine parameters (including scanning strategies) shall be fixed to establish the so-called "machine baseline parameters" to be used for all following builds. The machine shall be used in its calibrated state, keeping constant all settings, to guarantee performance repeatability. A certificate indicating the machine conforms to baseline parameters shall remain effective until the machine requires a new qualification. For some applications even more stringent standards are available. As an example, for space applications,

standards impose that each machine shall be used in its calibrated state not only avoiding any change of process parameters and scanning strategies, but also with all environmental and operational conditions kept fixed and using only virgin powders in any build (NASA, 2017a, 2017b). Therefore, assumption ii) applies to the most relevant industrial uses of metal AM technologies for the production of series of complex and innovative products. In this framework, there is currently a lack of adequate quality modelling and monitoring tools. Extensions of the proposed approach could be considered to deal with heterogeneous conditions as well. To this aim, transfer learning methodologies could be possibly used (Tsung et al., 2018).

A lattice structure can be represented by an array composed of $I \times J \times K$ unit cells placed side by side in the X and Y directions, and stacked on top of one another in the Z direction, in a regular grid. Without loss of generality, we consider unit cells with a cubic envelope the side length of which is l. We also assume that all the unit cells in the structure have the same as-designed geometry and no incomplete or partial cells are included. Under these assumptions, a lattice structure can be depicted as shown in Fig. 5. Referring to additively manufactured structures, hereafter the Z direction indicates the build direction, i.e., the direction along which material is added on a layer-by-layer basis to produce the part.
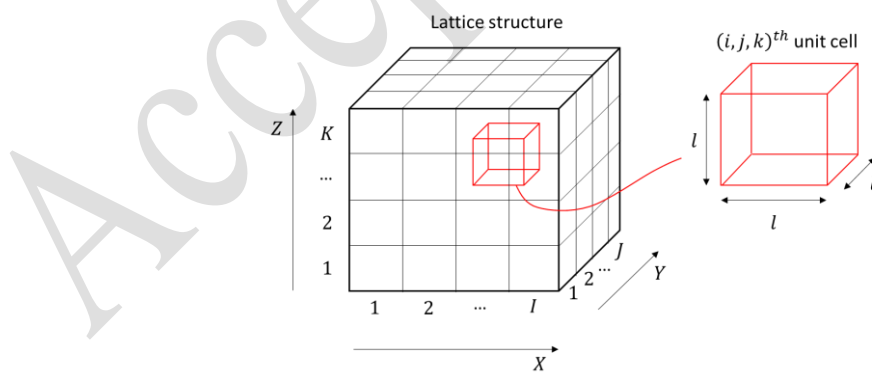
Fig. 5 – Schematic view of a lattice structure composed of $I \times J \times K$ unit cells

In the framework of additive manufacturing processes, the standard format for representing both the as-designed and as-built geometries is the STL format (Standard Triangulation Language) and this

format is used in this study, too.

The underlying idea of the proposed methodology consists of modelling the deviation between the as-built and the as-designed geometry for each unit cell of a lattice structure and using a statistical monitoring scheme to determine whether one or more unit cells exhibit an out-of-control geometrical distortion compared to the natural variability of the deviations from the as-designed shape in the entire structure.

The method can be applied to model and analyse the cell-to-cell variability in one single part, or to monitor the stability over time of within-part and part-to-part variability in a production series. For sake of clarity, the former application is presented first. The extension to a series production framework is discussed in Sub-section 4.6.

The method can be schematized as shown in Fig. 6, where, starting from the as-built and as-designed geometries of the same part, six sequential steps are envisaged. These steps are described and discussed in Sub-sections 4.1 – 4.5.
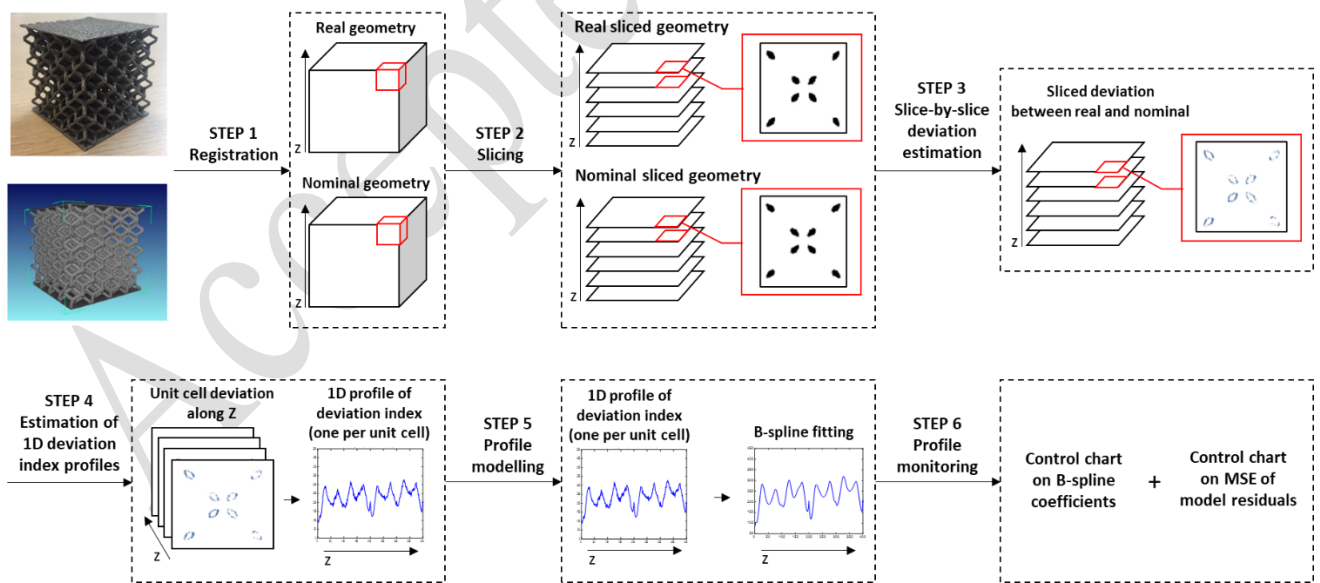
Fig. 6 – Overall scheme of the proposed methodology

4.1 3D shape registration

In order to estimate the deviation between the as-built and as-designed geometry, a registration operation is needed. Various methods have been proposed so far for registration purposes of 3D shapes that are applicable to meshes in STL format, including semi-automatic and fully automatic methods (Senin et al., 2013; Rusinkiewicz and Levoy, 2001; Holz et al., 2015). In this study, a semi-automatic alignment approach was applied, which envisages a two-stage procedure after placing the as-built and the as-designed geometry within a common coordinate system. The first stage consists of first rough registration based on landmarks defined by the operator. The second stage consists of fine registration based on the iterative closest point (ICP) algorithm (Rusinkiewicz and Levoy, 2001) that minimizes the alignment error between the two meshes applying a combination of rigid rotation and translation operations iteratively. The ICP algorithm has become the de-facto standard for fine registration of point clouds in various applications, but several variants have been proposed so far (Rusinkiewicz and Levoy, 2001; Senin et al., 2013). In this study we refer to the algorithm presented in Pulli (1999) and implemented in the open source Meshlab software (Callieri et al., 2003), which exploits a point-to-plane error metric (additional details can be found in Rusinkiewicz and Levoy, 2001). This algorithm has been widely used in additive manufacturing applications (e.g., for range map alignment of 3D scanned surfaces and dimensional compliance controls), and it has been found to be robust in the presence of complex shapes containing many kinds of surface features (Rusinkiewicz and Levoy, 2001).

It is worth noticing that the final spatial pattern of deviations between the as-built and as-designed geometries will consist of two contributions, i.e., the actual deviation caused by the inaccuracy and intrinsic signature of the manufacturing process, and the residual alignment error. Section 6.1 presents an assessment of the registration algorithm applied to our real case study. Future studies will possibly consider monitoring the registration coefficients together with the shape model parameters, thereby extending the approach proposed by Grasso et al. (2016) for statistical quality monitoring of functional data.

4.2 Pre-processing and slicing of the 3D geometry

Rather than computing the deviation between the as-built and as-designed geometries in three-dimensional space, the proposed approach envisages a slicing operation of both geometries analogous to the same operation needed to generate the build file for 3D printing of the part.

The as-built and as-designed geometries are sliced into a series of parallel cross-sections that are spaced apart at a fixed distance h. This allows one to compute the value of a given deviation index in each slice, i.e., at different levels along the build direction, leading to a representation of the deviation between the two geometries in a functional form, i.e., a deviation profile as a function of the Z coordinate. This yields a synthesis of the 3D deviation mapping in a 1D representation, which can be modelled by means of 1D functional data analysis methods (Ramsay, 2004). In this study, we set the spacing h equal to the layer thickness used to 3D print the part.

The as-designed geometry, represented in STL format, can be sliced into a vector graphics representation, which is then converted into bitmap images the maximum spatial resolution of which is limited by the slicing software. The x-ray CT reconstruction is first pre-processed by setting a threshold for voxel intensities to maximize the distinction between the solid part and the surrounding atmosphere. The resulting voxel representation is then sliced into bitmap images the maximum spatial resolution of which is limited by the original voxel size. In order to enable a pixel-wise comparison between each pair of images, a rescaling operation is applied to set an equal number of pixels per unit length in both the images. The final image resolution and the uncertainty sources related to the pre-processing phase are expected to contribute to the natural variability of the deviation index as nuisance factors.

A sliced representation of each unit cell is easily obtained by dividing each slice into $I \times J$ images. Let s be the spatial resolution of both as-built and as-designed geometry reconstructions: each unit cell is sliced into n 2D images of size $p \times p$ pixels, where $n = l/h$ and $p = l/s$, with $l\ being$ the side of the cubic envelope that encloses the cell.

The zth slice, with $z = 1,2, \ldots, n$, is a binary image, in which the intensity of the $(u, v)^{th}$ pixel, for $u = 1, \ldots, p$ and $v = 1, \ldots, p$, is such that $i_{u,v,z} = 0$ (black) if it is a foreground pixel (where there is material) and $i_{u,v,z} = 1$ (white) if it is a background pixel (where there is no material). This applies not only to the as-designed geometry but also to the as-built one gathered via x-ray CT as well. Indeed, the grey levels that correspond to x-ray attenuation are lost when an STL representation of the CT scanned geometry is extracted.

4.3. Estimation of the deviation index

Thanks to the registration operation, it is possible to compare the 2D image of the as-built geometry of each unit cell with the as-designed one, slice by slice. Given a pair of images that correspond to the zth slice of the as-designed cell and the zth slice of the as-built cell, let $i_{u,v,z}(as.\,designed)$ and $i_{u,v,z}(as.\,built)$ be the intensities of $(u, v)^{th}$ pixel in the as-designed slice and in the as-built slice, respectively. A superimposition of these two images leads to four possible regions of interest:

- Region 1: consists of all pixels in which both $i_{u,v,z}(as.\,designed) = 0$ and $i_{u,v,z}(as.\,built) = 0$, i.e., pixels where material is present in both the images.

- Region 2: consists of all pixels in which both $i_{u,v,z}(as.\,designed) = 1$ and $i_{u,v,z}(as.\,built) = 1$, i.e., pixels that correspond to the background in both the images.

- Region 3: consists of all pixels in which $i_{u,v,z}(as.\,designed) = 0$ and $i_{u,v,z}(as.\,built) = 1$, i.e., pixels where material is present in the as-designed slice but not in the as-built slice (i.e., less material has been produced than indicated in the CAD model).

- Region 4: consists of all pixels in which $i_{u,v,z}(as.\,designed) = 1$ and $i_{u,v,z}(as.\,built) = 0$, i.e., pixels where material is present in the as-built slice but not in the as-designed slice (i.e., more material has been produced than indicated in to the CAD model).

The union of region 3 and region 4 represents the deviation between the as-built and as-designed geometry. Fig. 7 shows an example of corresponding as-built and as-designed slices and their deviation (the images refer to the real case study described in Section 3).
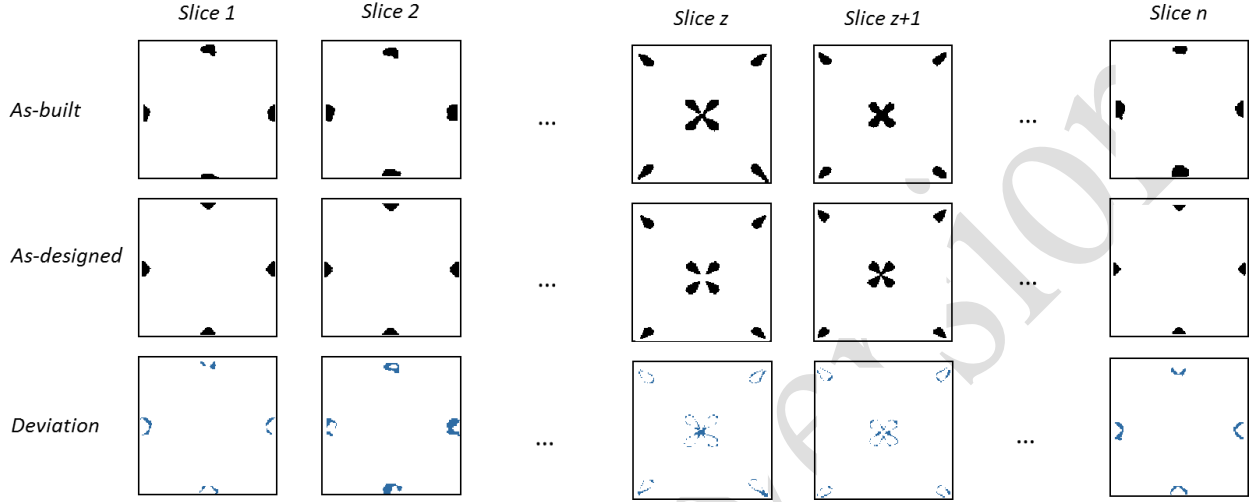
Fig. 7 – Example of as-built (top row) and as-designed (central row) slice images at different z heights with the corresponding deviation (bottom row)

The overall number of pixels that belong to the union of region 3 or region 4 is the number of pixels for which $i_{u,v,z}(as.built) - i_{u,v,z}(as.designed) \neq 0$. Therefore, the deviation index for the $(i,j,k)^{th}$ unit cell as a function of the level along the Z coordinate can be defined in pixel-wise terms as follows:

$$\delta_{i,j,k}(z) = \sum_{u=1}^{p} \sum_{v=1}^{p} \mathcal{I}(i_{u,v,z}(as.built) - i_{u,v,z}(as.designed) \neq 0)_{i,j,k},$$

$$i = 1, \dots, I, j = 1, \dots, J, k = 1, \dots, K, z = 1, \dots, n$$

(1)

where $\mathcal{I}(\cdot)$ is the indicator function, that is 1 if the condition in brackets is true and 0 otherwise.

In this study, we present the proposed methodology by using the deviation index $\delta_{i,j,k}(z)$ defined in Eq. 1. Nonetheless, the same approach can be applied to different definitions of the deviation between the as-built and as-designed geometry.

It is worth mentioning that the deviation between the as-built and as-designed geometry can include not only a different shape of the sliced geometry, but also the possible lack of material, i.e., pores within the struts, which may have detrimental effects on the mechanical performance of the structure. Since the deviation index is computed as a pixel-wise difference, it is naturally suitable for taking into account the presence of pores in the struts as well.

4.4 Profile modelling

The deviation index $\delta_{i,j,k}(z)$ can be represented as a discrete 1D profile, where the zth value measures the deviation between the as-built and as-designed geometry in the zth slice along the build direction of the $(i,j,k)^{th}$ unit cell (Fig. 8).
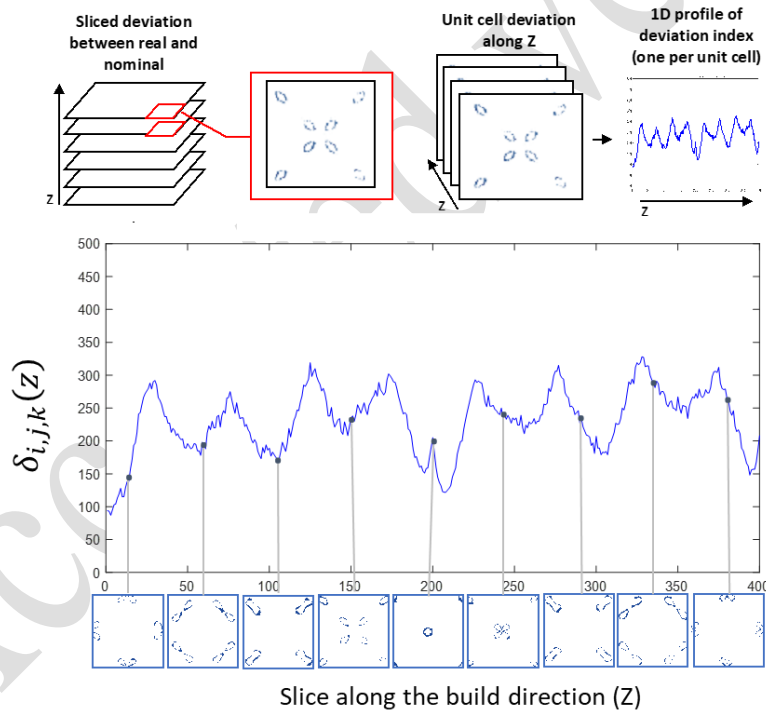
Fig. 8 – From slice-by-slice deviation to the 1D deviation index profile

In order to analyse the natural variability of the deviation index profiles and to identify anomalous patterns, discrete profiles can be converted into a functional form. This allows one to design a control-charting scheme grounded on the functional data analysis (FDA) framework. To this aim, we propose a representation of the functional profiles on a cubic B-spline basis (Ramsay, 2004) as follows:

$$\hat{\delta}_{i,j,k}(z) = \sum_{q=1}^{Q+L-1} c_{i,j,k,q}\Phi_q(z,\boldsymbol{\tau}), \qquad i = 1,\dots,I, j = 1,\dots,J, k = 1,\dots,K, z = 1,\dots,n \qquad (2)$$

where $Q = 4$ is the order of the B-spline functions (cubic splines), L is the number of subintervals separated by $L - 1$ interior knots, $\boldsymbol{\tau}$ is the knot sequence $\boldsymbol{\tau} = \{\tau_l, l = 1,2,\dots,L\}$, $c_{i,j,k,q}$ are the B-spline coefficients for the $(i, j, k)^{th}$ unit cell, and Φ_q are the B-spline basis functions. The B-spline basis is particularly suitable for fitting the deviation index profiles as they may present a discontinuity of first and second derivates at levels along the Z axis at which the trabecular shape exhibits abrupt changes (e.g., where struts connect to junctions). Indeed, by placing multiple coincident knots in which a discontinuous derivative occurs, this discontinuity can be properly captured by the B-spline model.

The knot sequence $\boldsymbol{\tau}$ can be defined in different ways, e.g., by manually selecting the knots' locations or by setting an appropriate number of equispaced knots leading to a reasonable balance between the CPU time and goodness-of-fit. More advanced knot selection strategies have been proposed in literature so far (e.g., Goldenthal and Bercovier, 2004, Zhou and Shen, 2001; Molinari *et al*., 2004, Sangalli et al., 2009). In this study, the knot sequence was determined starting from an initial sequence of knots placed at the discontinuities of the as-designed geometry, and iteratively adding intermediate knots until a knee in the mean squared error (MSE) of the B-spline model residuals was found. The same knot sequence can be applied to deviation index profiles for unit cells of the same type and dimension.

4.5 Profile monitoring

Profile monitoring represents a category of statistical process monitoring methods suitable for dealing with profile data (Woodall, 2007). Various authors have proposed monitoring schemes for profiles fitted by means of a spline basis. First seminal works (Gardner et al., 1997, Williams et al, 2007)

proposed the computation of metrics, e.g., the quadratic error, the absolute error, the maximum error, etc., to be monitored via univariate or multivariate control charts. Chuang et al. (2013) proposed a monitoring method that combined a B-spline model with a location control chart, i.e., a chart where the control region is represented by a confidence band around the in-control profiles. A different approach (Gomaa and Birch, 2019; Grasso et al., 2016; Hadidoust et al., 2015) consists of using a multivariate control chart to monitor the multivariate distribution of the B-spline model parameters. One additional control chart can be used to detect shifts in the model residuals too. In this study, this latter approach is followed.

The methodology works as follows:

- Once a lattice structure has been produced and measured via x-ray CT, the previously described steps are performed to estimate the deviation index for each unit cell and fit the B-spline model to the $N = I \times J \times K$ deviation index profiles.

- Let $N = I \times J \times K$ be the number of unit cells in the structure and let $i' = 1,2,\dots,N$ be the unit cell identifier that univocally associates each cell with a number in the range $[1, N]$ according to a pre-defined order. The B-spline coefficients of all the deviation index profiles can be re-arranged into a $N \times (Q + L - 1)$ matrix $\mathbf{C}$ so that the $(i', q)^{th}$ element of the matrix is $\mathbf{C}_{i',q} = c_{i,j,k,q} = c_{i',q}$. This matrix will be augmented by one column to include the sample mean of the i'-th deviation index profile $\bar{\delta}_{i,j,k} = \bar{\delta}_{i'}$. This allows monitoring not only the shape of the profiles, but also their average value. The resulting data matrix used to design the control charts is the following $N \times (Q + L)$ matrix:

$$
\mathbf{X} = \begin{bmatrix} c_{1,1} & \cdots & c_{1,Q+L-1} & \bar{\delta}_1 \\ c_{2,1} & \cdots & c_{2,Q+L-1} & \bar{\delta}_2 \\ \cdots & \cdots & \cdots & \cdots \\ c_{N,1} & \cdots & c_{N,Q+L-1} & \bar{\delta}_N \end{bmatrix} = \begin{bmatrix} x_1^T \\ x_2^T \\ \cdots \\ x_N^T \end{bmatrix}
\tag{3}
$$

- For each deviation index profile, the mean squared error (MSE) of the B-spline model residuals

is estimated too. The values are stored in the $N \times 1$ vector $\boldsymbol{MSE}$, where:

$$MSE_{i'} = \frac{1}{N - (Q + L - 1)}(\delta_{i'} - \hat{\delta}_{i'})^T(\delta_{i'} - \hat{\delta}_{i'}), \qquad i' = 1,2,\dots \qquad (4)$$

- Two control charts can be designed. First, an Hotelling's T^2 control chart based on the data matrix $\mathbf{X}$ can be used to detect outlying patterns in the deviation index profiles, so that:

$$T_{i'}^2 = (\boldsymbol{x}_{i'} - \overline{\boldsymbol{x}})^T \mathbf{S}^{-1}(\boldsymbol{x}_{i'} - \overline{\boldsymbol{x}}), \qquad i' = 1,2,\dots, \qquad (5)$$

where $\mathbf{S}$ is the variance-covariance matrix of the $\mathbf{X}$ data matrix, and $\overline{\boldsymbol{x}}$ is the sample mean of vectors $\boldsymbol{x_1}, \dots, \boldsymbol{x_N}$. The upper control limit (UCL) for the T^2 control chart, to be used in Phase I, is defined as follows:

$$UCL_{T^2} = \frac{(N-1)^2}{N}\beta_{\alpha,\frac{Q+L}{2},\frac{N-Q-L-1}{2}} \qquad (6)$$

where: $\alpha = \alpha'/2$ is the Type I error computed by using the Bonferroni's correction (Montgomery, 2008), in which α' is the family-wise Type I error; $\beta_{\alpha,\frac{Q+L}{2},\frac{N-Q-L-1}{2}}$ is the $100(1-\alpha)\%$ percentile of a beta distribution with $\frac{Q+L}{2}$ and $\frac{N-Q-L-1}{2}$ degrees of freedom.

The second is a standard Shewhart's control chart for the MSE statistic.

In the presence of one single lattice structure, the use of the proposed control charts is analogous to the Phase I retrospective use of control charts in traditional statistical process control. The objective consists of signalling an alarm when one or more unit cells exhibit an outlying pattern in terms of deviation from the as-designed geometry. The use of a T^2 control chart rather than a MEWMA or MCUSUM control chart is mainly due to the need to also detect a nonpersistent shift. As a matter of fact, shifts can also happen occasionally at a given location without having to remain persistent along

the z direction.

It is worth noting that, differently from traditional control charts, the X-axis of the chart is not a temporal axis, but represents a location. This kind of control chart has been referred to as a "spatial chart" in literature (Megahed, et al., 2011). Examples of spatial control chart methods were presented by Lin and Chiu (2006), Lin (2007a, 2007b), and Lin et al. (2008). In our study, the value on the X-axis of the control charts is the identifier of the unit cell within the lattice structure, i.e., $i' = 1, \dots, N$. This implies that, "by-construction", there is univocal correspondence between each 1D deviation profile, i.e., each plotted point in the control charts, and each unit cell in the lattice structure. Thus, whenever an out-of-control situation is signalled, the corresponding unit cell location in the structure can be automatically identified. The T^2 and MSE control charts are independent from the data sorting, and hence they yield the same result for any possible ordering of the unit cells and corresponding deviation index profiles. Therefore, they are suitable for use as "spatial" control charts for the detection of outlying cell geometries in the lattice structure.

4.6 Moving from one-of-a-kind to series production

The method described in previous sub-sections refers to its possible use to detect anomalies affecting one or multiple unit cells of one single lattice structure. This approach applies to parts where the unit cell geometry regularly repeats within the entire structure. Grounding on the assumption that all unit cells are produced with the same process parameters and with the same geometry, a stable (in-control) process is expected to produce 1-D deviation profiles whose natural variability is random from cell to cell. On the contrary, any systematic or outlying variation affecting one or multiple unit cells is expected to be a possible indication of an out-of-control structure. Thus, by applying the proposed profile monitoring approach to the N deviation profiles associated to N unit cells of the same part, it is possible to signal an alarm whenever a geometrical or dimensional anomaly is present in one or more unit cells. This approach is suitable for quality modelling of one part at a time, and it is therefore directly applicable to one-of-a-kind structures.

This procedure can be extended to the analysis of cell-to-cell variability even in the presence of multiple copies of the same structure with the same as-designed geometry. Indeed, a set of M parts produced under in-control process conditions can be collected, each one consisting of N unit cells. The proposed profile monitoring approach can be applied by considering all $N \times M$ deviation profiles collected during the design phase as replicates of the same profile pattern realization. In this case, the $N \times M$ deviation profiles can be used to estimate the control limits for the T^2 and MSE control charts. A retrospective Phase I use of the control charts can be used to check whether the M parts used to design the control charts were actually in-control or not. In Phase II, for every newly manufactured lattice structure of the same type and geometry, the T^2 and MSE statistics are computed for each unit cell with a sample size $n = 1$, since unit cells are treated as individual observations. An example of this approach is discussed in Section 6.3.

Despite being suitable to detect local anomalies affecting even one single unit cell of a part, this approach is not suitable to distinguish within-part and between-part variations. To this aim, the proposed approach can be further extended as follows. A set of M parts produced under in-control process conditions, each one consisting of N unit cells, can be collected and used to design a multivariate control charting scheme with sample size $n = N$. This implies that each lattice structure consists of a rational subgroup, allowing the design of a T^2 control chart with $n = N$ combined with a control char for multivariate variability, e.g., the Wishart control chart (Montgomery, 2008). In this extended version of the proposed approach, the Hotelling's T^2 control chart is used to detect shifts in the mean deviation from the nominal geometry from one part to another, whereas the Wishart control chart allows monitoring the stability of the within-part variability over time. For the definitions of T^2 and Wishart control charts we refer the reader to Montgomery (2008). This extended approach is less sensitive to local anomalies, being based on aggregated statistics, but it is suitable to detect global shifts of the mean together with unnatural changes in the within-part variability. An example of this approach is discussed in Section 6.4.

5. Simulation study

A simulation study was performed to assess the effectiveness of the proposed approach in detecting local geometrical distortions and to compare its performance against a benchmark competitor representative of industrial practices. Starting from the real x-ray CT reconstruction of specimen A, local geometrical distortions were simulated by injecting an artificial modification of the images that represent the as-built geometry after the 3D mesh slicing operation. Both the as-designed and as-built geometries were sliced at $h = 0.025$ mm centres, equal to the layer thickness applied in the LPBF process. This yielded a number of slices for each unit cell equal to $n = 400$.

In order to make the injection of local anomalies realistic, we referred to previous studies on the effect of local geometrical distortions on the mechanical performance of lattice structures. In particular, Liu et al. (2017) pointed out that both oversizing and under-sizing single struts and junctions might influence the type of failure mechanism. Based on this, a scale factor, hereafter denoted by sf, was applied either to one single strut or to one single junction to simulate a local oversizing effect as shown in Fig. 9. The severity of the simulated distortion was controlled by varying the scale factor in the range $sf \in [1, 2]$, where $sf = 1$ corresponds to the original image, without distortion.
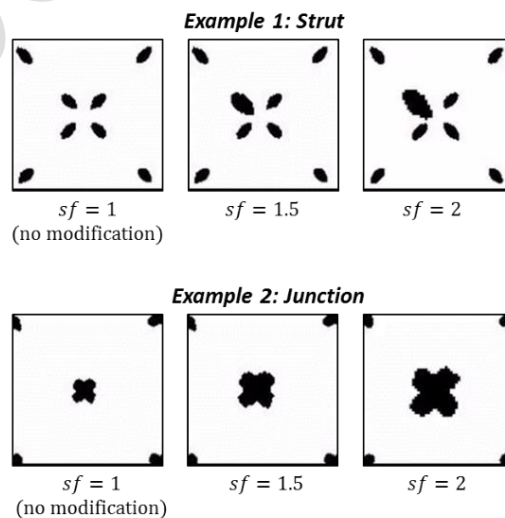
Fig. 9 – Example of simulated oversizing effect in one single strut (top panel) and in one junction (bottom panel) for different scale factor levels

The simulation analysis was performed by injecting the artificial oversizing effect in randomly selected struts and junctions and evaluating the Type II error as a function of the scale factor.

The control charts were designed by removing the profile data corresponding to the 52-nd unit cell of specimen A with the actual distortion defect.

In the absence of benchmark methods for statistical quality monitoring of lattice structures in literature, as a competitor approach we considered a method that is representative of a "simple" industrial practice. It relies on monitoring a commonly used quality index for lattice structures. Various authors investigated the geometrical accuracy of lattice components by measuring synthetic descriptors (Liu et al., 2017; Dallago et al., 2019; Han et al., 2018; Melancon et al., 2017; Van Bael et al., 2011). Among them, two examples of quality metrics commonly used are the average distance between each pair of struts, called *average pore size*, and the ratio between the empty volume and the overall envelope volume of the unit cell, also called *as-built porosity* (Van Bael et al., 2011). In this study, the latter index was considered. A competitor statistical quality monitoring method was developed by designing a univariate Shewhart's control chart to the as-built porosity of the cell. This approach is deemed representative of a solution that is easily implementable by practitioners in the presence of such complex structures.

The average operating characteristic curves for our proposed approach and the competitor method in the two simulated scenarios, i.e., the one with simulated oversizing of the strut and the one with simulated oversizing of the junction, are shown in Fig. 10.

Fig. 10 shows that the proposed method is effective in detecting even small deviations (with $sf < 1.3$) that are hardly visible to the naked eye when the 3D mesh is inspected. The fact that the proposed method outperforms the competitor is mainly due to the "local" nature of our profile monitoring technique, which takes into account the evolution of the deviation index along the build direction, rather than considering one single synthetic porosity value.
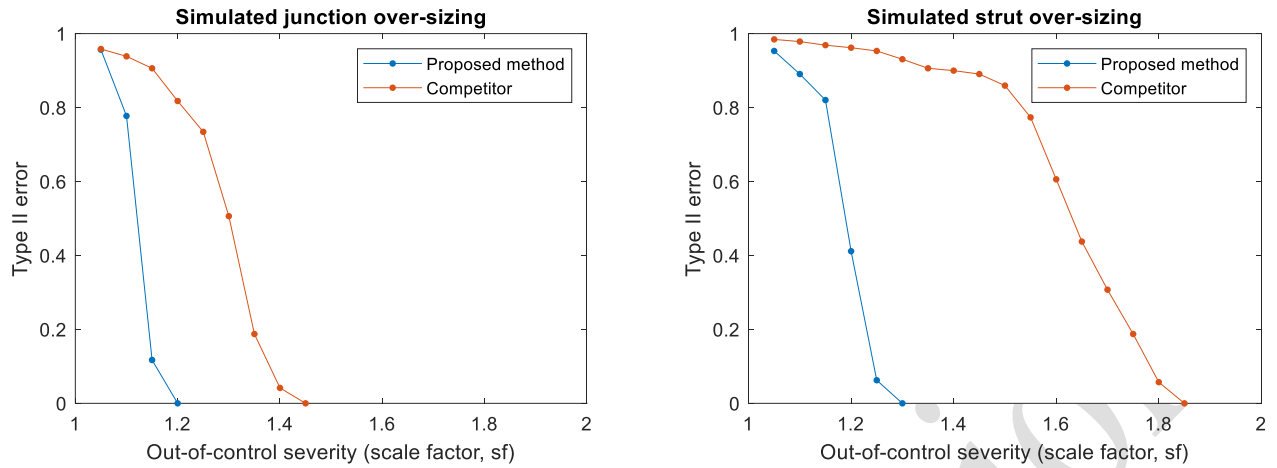
Fig. 10 – Operating characteristic curves for the proposed approach (blue lines) and the competitor method based on the as-built porosity index (orange lines) for simulated junction oversizing (left panel) and simulated strut oversizing (right panel)

Oversizing in the junction is easier to detect than oversizing in one single strut, as it yields a larger absolute deviation from the as-designed geometry. When the artificial defect is injected into one single strut, the gap between the performance of our proposed method and that of the competitors increases for the same reason, i.e., a more local distortion yields a smaller effect on the synthetic porosity index, making our proposed approach more effective.

This analysis shows that the proposed method may be a suitable tool for keeping the quality of complex lattice structures under control, and for signalling local out-of-control deviations from the CAD model, which may translate into detrimental effects in terms of final performance.

6. Real case study analysis

6.1 Assessment of the alignment algorithm

In order to estimate the validity of the registration operation and to evaluate the settings of the registration algorithm, two analyses were performed. The first analysis consisted of creating two identical copies of the nominal (as-designed) shape and aligning one with the other with different choices of the landmarks used for the first rough registration step. This first analysis allowed us to evaluate the minimum number of ICP iterations needed to guarantee the convergence of the algorithm

for different initial misalignment errors and to evaluate the impact of different landmark choices on ICP convergence.

Three different choices of the number of landmarks were considered. For each choice, two sets of landmarks were selected on two opposite sides of the lattice structure. On each side, the number of landmarks was equal to $n_{land} = 4, 8$ and 16 respectively. Fig. 11a shows the location of the landmarks for each choice of n_{land}.
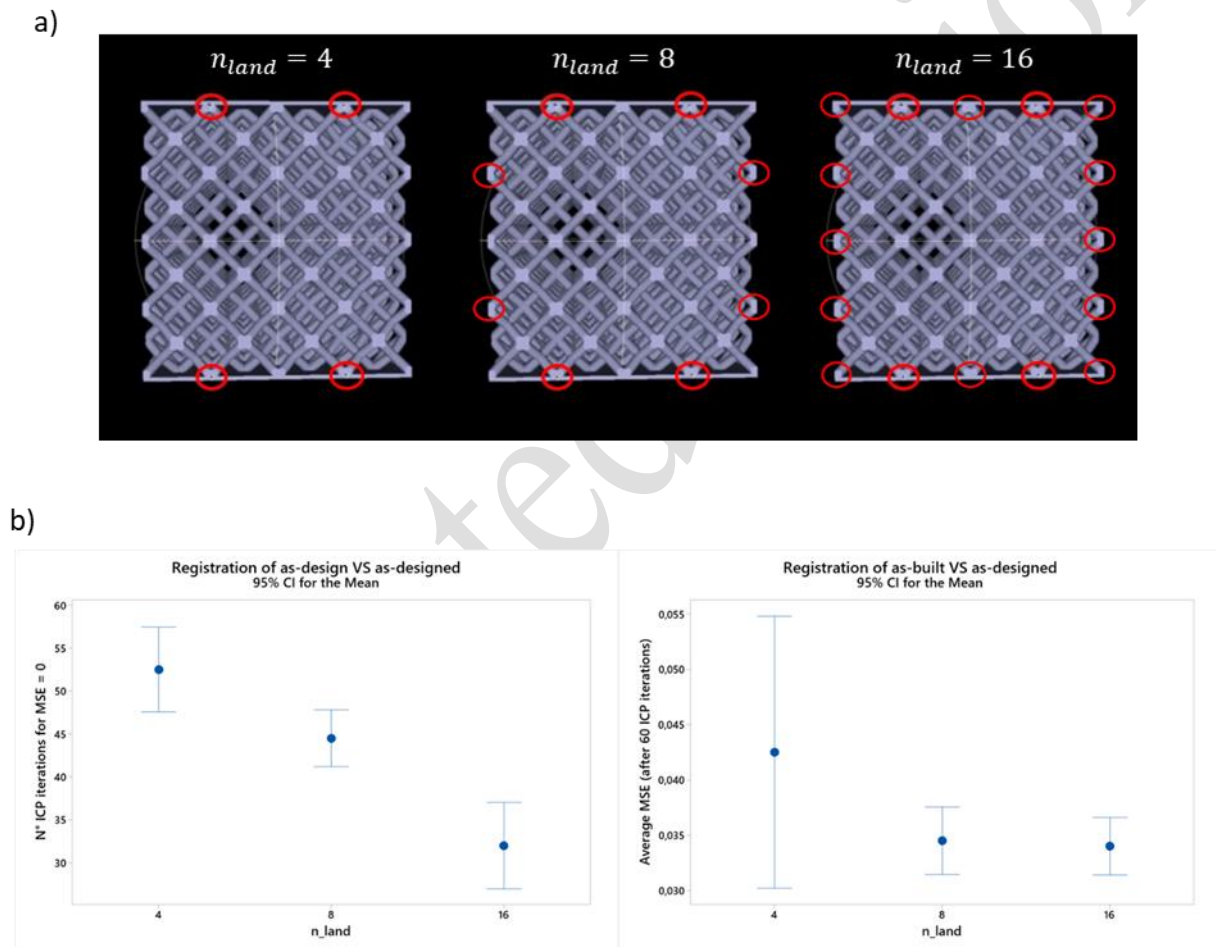
Fig. 11 – a) Example of landmark locations on one side of the lattice structure for different choices of n_{land}; b) Number of ICP iterations to achieve an average MSE = 0 when registering two copies of the as-designed shape (left panel) and average MSE after 60 ICP iterations when registering the as-built shape compared to the as-designed one (right panel)

The landmarks were placed at junctions along the external contour of the structure. For each landmark configuration, four trials were performed. In each trail, the location of landmarks on one copy of the shape was exactly the same as the other copy, but random initial misalignment conditions were

selected. For each trial, the residual misalignment error was estimated as the mean squared error (MSE) for each pair of corresponding landmarks. The Euclidean distance was used for estimating the MSE.

Fig. 11b (left panel) shows the 95% confidence intervals of the number of ICP iterations required to achieve an average MSE = 0 for each choice of n_{land}. Fig. 11b (left panel) confirms that increasing the number of landmarks caused a decrease in the number of iterations required. In the worst configuration, i.e., the one with $n_{land} = 4$, fewer than 60 iterations were needed to achieve a perfect registration of the two copies of the same shape.

By setting the number of ICP iterations at 60, the second analysis consisted of testing the same choice of landmarks in the registration between the as-built and as-designed shapes. The average MSE was computed by varying the initial misalignment error (also in this case four trials for each landmark condition were performed). Fig. 11b (right panel) shows that with $n_{land} = 4$, the dispersion of the average MSE was larger than with $n_{land} = 8$ or $n_{land} = 16$. Moreover, there was no statistically significant difference in the use of either eight or sixteen landmarks on the final MSE. A similar analysis was repeated with larger numbers of ICP iterations, but no statistical improvement of the average MSE was observed.

Generally speaking, a quantitative determination of the actual registration error can be obtained only for simulated data, where the ideal position of the points of the mesh is explicitly designed in the simulation (Senin et al., 2013). Indeed, the MSE is affected both by the residual misalignment and by the local differences between the as-built and as-designed shapes. However, the preliminary analysis presented here allowed us to assess the effect of different choices of landmarks. In particular, the configuration with $n_{land} = 8$ landmarks and 60 iterations of the ICP algorithm were selected and used in the following analysis. Keeping the settings for the registration algorithm of each analysed part fixed, the residual misalignment error will represent a nuisance term affecting the natural pattern and variability of the monitored deviation index profile.

6.2 Cell-to-cell variability analysis for one single lattice structure

The proposed method for within-part variability analysis and identification of local geometrical distortions was first applied to specimen A.

As mentioned in Section 4, a data-driven selection of the knot sequence was applied. Starting from knots placed at z levels where major modifications of the as-designed geometry take place, additional knots were iteratively added and the MSE for all B-spline model residuals was recorded. Fig. 12a shows the boxplots of the MSE values for the $N = 64$ unit cells of the lattice specimen corresponding to different knot sequences with an increasing number of knots, starting from a minimal know sequence with $L = 24$ knots. The sequence with $L = 49$ knots was eventually selected since the addition of further knots did not yield any significant reduction in the MSE of model residuals. The knot sequence is shown in Fig. 12b, where the correspondence between knot positions and salient features of the cell is highlighted (for sake of clarity one single deviation index profile is shown in Fig.12b, left panel).
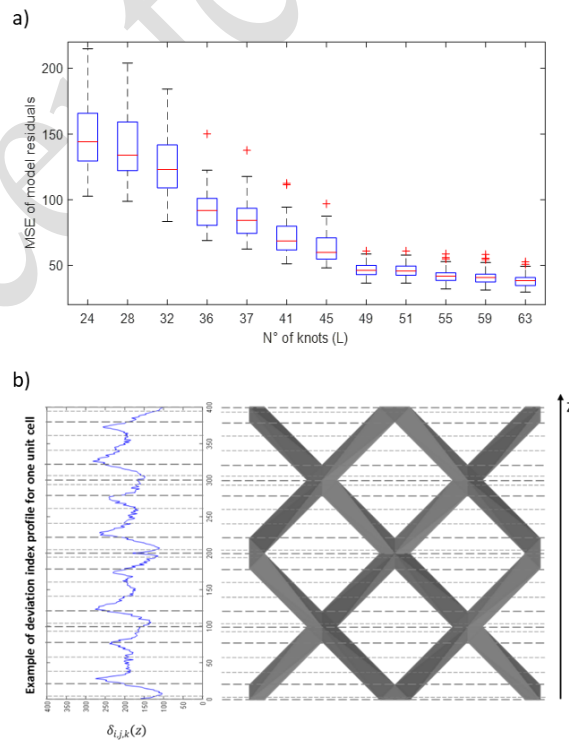
Fig. 12 – a) Boxplots of MSE values of B-spline model residuals for different knot sequences with an increasing number of knots; b) Example of knot placement in correspondence to salient features of the as-designed unit cell geometry (one deviation index profile is shown in the left panel)

Fig. 13 shows all the deviation index profiles for the $N = 64$ unit cells of lattice specimen A (top panel), the corresponding B-spline model fits (central panel) and the model residuals (bottom panel). The general pattern of the deviation index profiles can be regarded as a signature of the LPBF process with given process parameters for the selected dodecahedron lattice structure, with main discontinuities corresponding to the salient geometrical features of the unit cell.
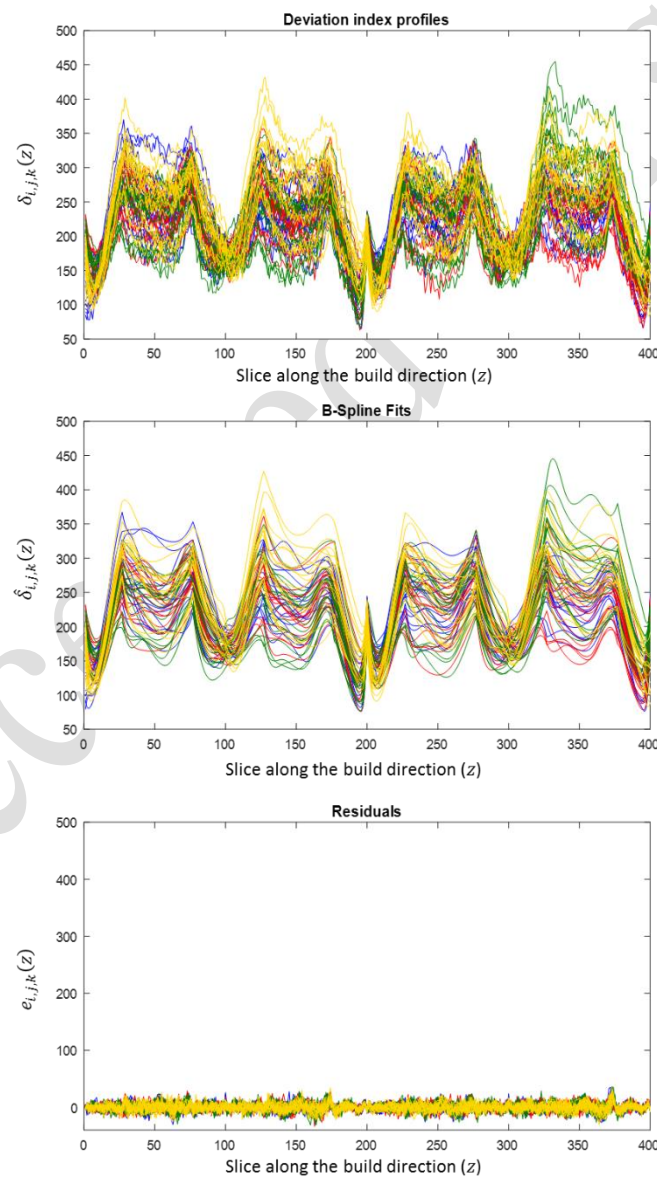
Fig. 13 – Deviation index profiles (top panel), B-spline model fits (central panel) and B-spline model residuals (bottom panel) for specimen A

The cell-to-cell variability is caused by small local variations as a result of the LPBF process itself. In particular the cell-to-cell variability was lower at the centre of junctions and it inflated where diagonal struts were produced. Indeed, since the main source of deviation between the as-built and as-designed geometries is a general oversizing of the former compared to the latter, the deviation is larger at z heights were more material was printed.

The control charts for within-part variability analysis are shown in Fig. 14, designed with family-wise Type I error $\alpha = 0.0027$.
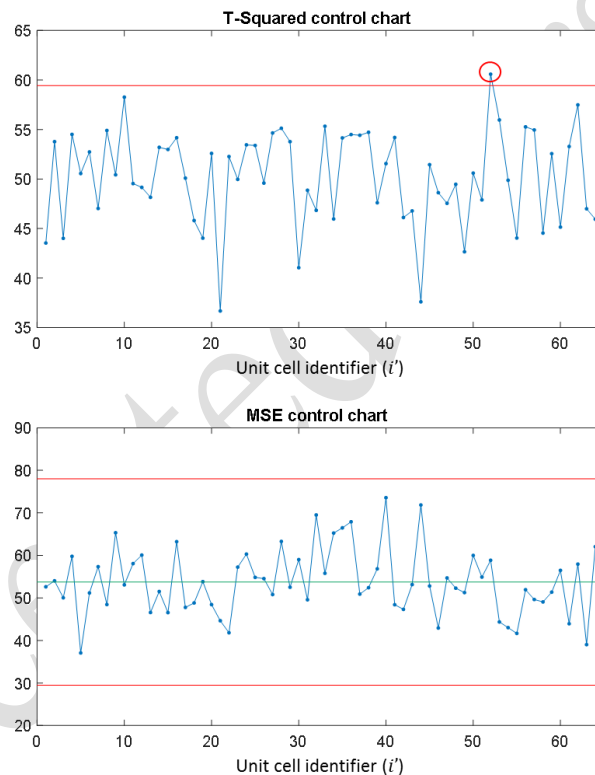
Fig. 14 – Control charts for within-variability analysis of specimen A

The T^2 control chart signals an out-of-control situation at the 52-nd unit cell. The visual inspection of the deviations between the two geometries on a slice-by-slice basis revealed that the as-built geometry exhibits a global over-sizing of struts and junctions in the 52-nd cell compared to the original CAD model (Fig. 15a). One possible cause for such deviation is non-uniform powder recoating in the very last layers due to a worn recoating unit that modified the local energy density

leading to a swelling of the structure. A few irregularities in the powder bed were observed at the end of the build.
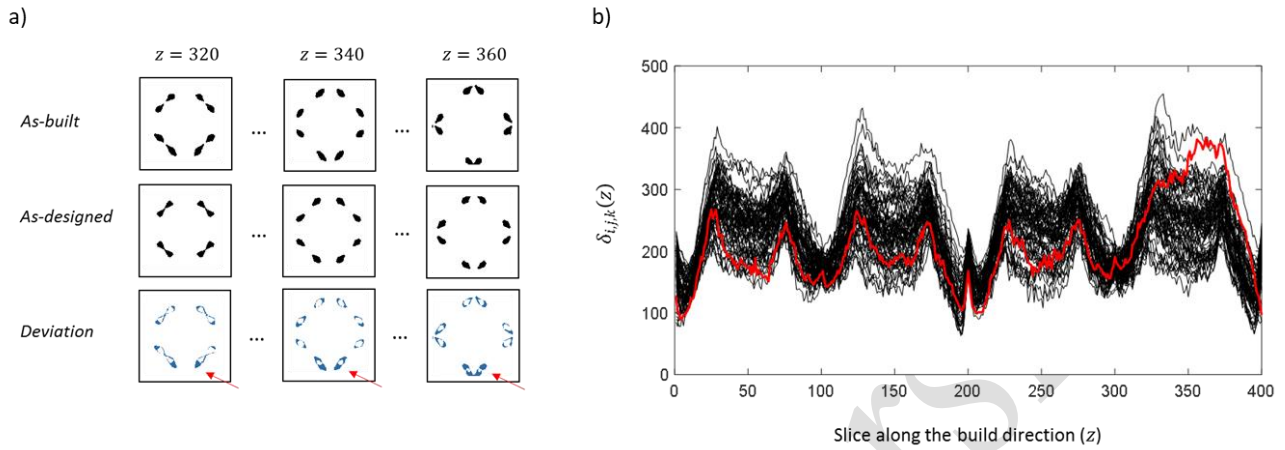
Fig. 15 – a) Examples of as-built, as designed and deviation images at the local distortion of the 52-nd unit cell belonging to specimen A signalled as out-of-control by the proposed control chart; b) Deviation index profile of the 52nd-unit cell of specimen A signalled as out-of-control (red curve) superimposed on all other profiles that belong to specimen A

The deviation index profile that corresponds to the unit cell signalled as out-of-control by the T^2 control chart is highlighted in Fig. 15b. In terms of 1D deviation index profile, this unit cell exhibits a different signature in the upper region, between slice $n = 325$ and slice $n = 375$, that is properly signalled by the control chart. It is worth noticing that this distortion may be hardly visible to the naked eye. Moreover, the as-built porosity of unit cells in specimen A range between 94.66% and 94.81%, and the as-built porosity of the 52-nd unit cell is 94.67%, which makes the geometrical distortion not detectable by looking at the synthetic porosity index of the cell. Therefore, the proposed method may provide practitioners with a novel tool for characterizing the natural variability of lattice structures in more depth, and for identifying the presence of local out-of-control distortions that may be critical for the functional performance of the component.

6.3 Cell-to-cell variability analysis for copies of the same structure

A simplified example is presented to highlight the possible use of the proposed approach for the analysis of part-to-part variability and statistical process monitoring when copies of the same product

are manufactured. As this is a simplified example, one single lattice specimen was used to design the control charts, i.e., specimen A, and the same control charts were then applied to the data from the second specimen, i.e., specimen B. The control limits estimated for specimen A were re-estimated by removing the deviation index profile that corresponds to the out-of-control cell with the local distortion defect. Fig. 16 compares the deviation index profiles for the unit cells of specimen A (left panel) and those for the unit cells of specimen B (right panel), whereas Fig. 17 shows the control charts designed based on $M = 63$ in-control unit cells of specimen A and applied to all the cells of specimen B (only Phase II control charts are shown).
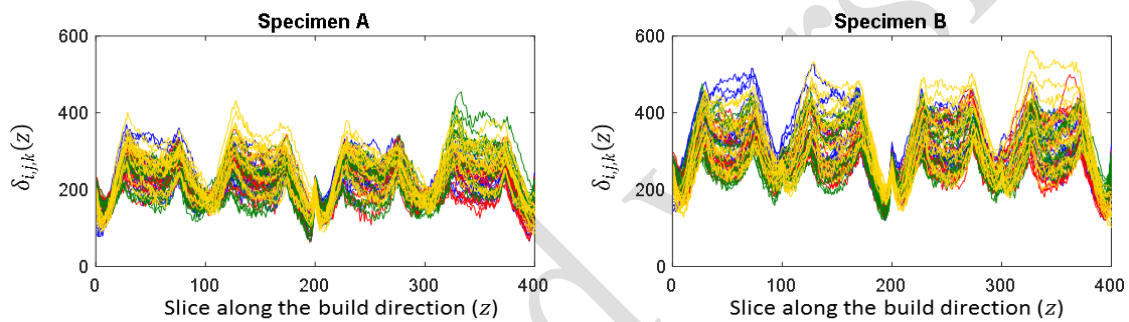
Fig. 16 – Deviation index profiles of unit cells that belong to specimen A (left panel) and specimen B (right panel)
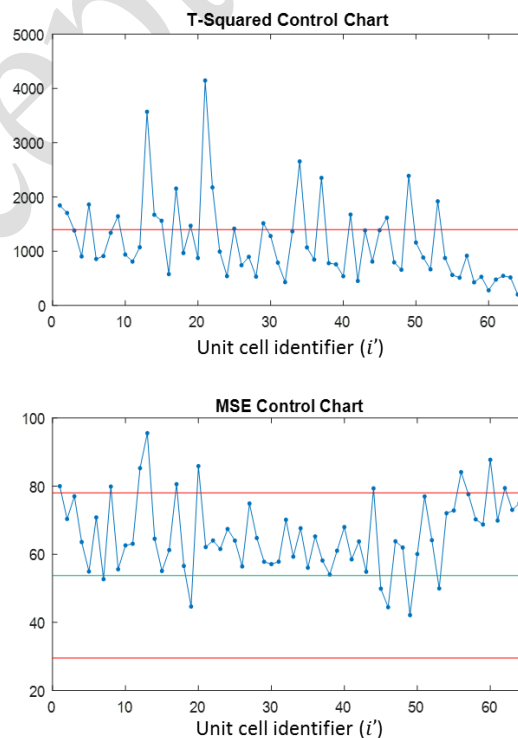
Fig. 17 – Phase II control charts applied to unit cells that belong to specimen B

Fig. 16 shows that, although the general patterns of the deviation index profiles repeat in the two copies of the same lattice structure, profiles that belong to specimen B have a larger mean value than those for specimen A, which corresponds to a more severe global oversizing effect in specimen B. Moreover, the cell-to-cell variability in specimen B is larger than that in specimen A. Such effects were induced by the lack of laminarity of the inert gas flow in the build area where the specimen B was produced, which was used to introduce on purpose a variation of geometrical and dimensional properties of the two specimens. The differences between the two copies of the same lattice structure are clearly identified by the proposed control charting method (Fig. 17), with about one third of unit cells signalled as out-of-control by the T^2 control chart and a sustained mean shift in the MSE control chart.

6.4 Extension to within-part and part-to-part variability monitoring

As mentioned in Section 4.6., the proposed approach can be used to monitor the within-part and part-to-part variability in a series production. Instead of using the unit cell as individual observation, each lattice structure can be treated as a rational subgroup with sample size, n, equal to the number of unit cells in the part, N. In order to show how this approach can be implemented in practise, real data from specimen A and B were used to artificially generate a large number of occurrences representing copies of the same structure. More specifically, $M = 30$ random replicates of a B-spline coefficient vector of size $p = Q + L - 1$ were drawn from a multi-normal distribution with mean $\boldsymbol{\mu}_A$ equal to the sample mean of specimen A's B-spline coefficients, and variance-covariance matrix $\boldsymbol{\Sigma}_A$ equal to the sample variance-covariance of the same coefficients. These M samples were used for the design of T^2 and Wishart control charts. Additional 50 samples were drawn from the same multi-normal distribution (25 samples) and from the multi-normal distribution with mean $\boldsymbol{\mu}_B$ and variance-covariance matrix $\boldsymbol{\Sigma}_B$ equal to the sample mean and variance-covariance of specimen B's B-spline coefficients (25

samples), respectively. The resulting control charts are shown in Fig. 18 (control limits were estimated as empirical percentiles of Phase I monitoring statistics).

Fig. 18 shows that lattice structures simulated from sample statistics of specimen B exhibit an evident shift of both the mean and the variability with respect to structures simulated using the sample statistics of specimen A. This effect is much more evident in Fig. 18 than in Fig. 17 because the T^2 and Wishart control charts are designed with a large sample size ($n = 64$) that leads to a very high power in the detection of a global shift like the one characterizing specimen B. Nevertheless, the T^2 and Wishart statistics computed in this way are expected to be less sensitive to very local anomalies affecting only one unit cell or a few of them. In that case, a control charting scheme like the ones discussed in previous sections could be more effective.

Fig. 18 represents an example of how the proposed approach can be combined with multivariate control charts with rational subgroups to move from one-of-a-kind part monitoring to process monitoring of series productions.
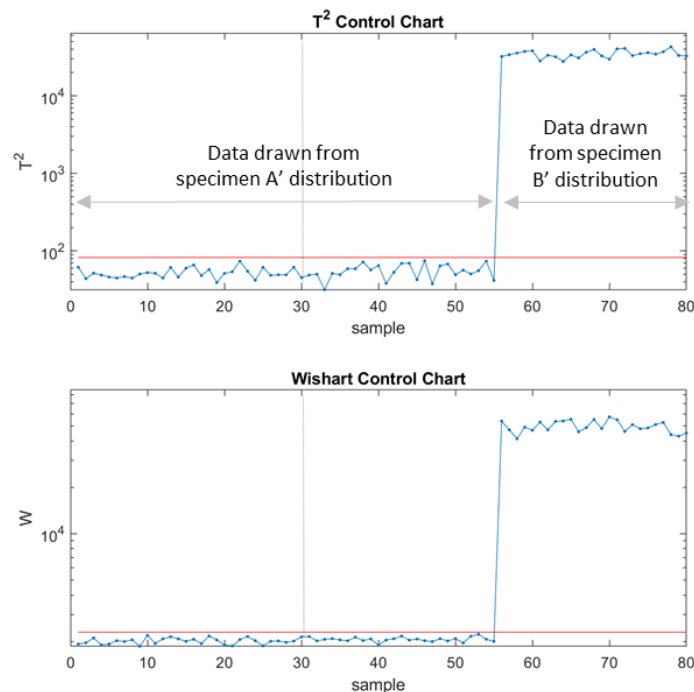
Fig. 18 – T^2 and Wishart control charts for series production monitoring of within-part and part-to-part variability (the vertical dotted line separates Phase I from Phase II)

7. Conclusions

Novel types of complex shapes are becoming more and more widespread in industry thanks to new manufacturing technologies and production paradigms. This causes industrial statistics practitioners to face new challenges for quality inspection and monitoring of discrete manufacturing processes. Lattice structures are novel shapes with a great potential for innovative applications in various industrial sectors, e.g., aerospace, biomedical, automotive, etc. However, one major issue regards the lack of statistical quality monitoring methodologies that are suitable for assessing the conformity of individual parts, and for keeping the production process under control statistically. From an industrial perspective, it is particularly critical to determine the variability of the geometrical properties from cell to cell, as such variability may have detrimental effects on the functional performances of the structure. This study presented a first approach aimed at tackling these challenges. Relying on a geometrical reconstruction of the part produced using X-ray CT, the proposed methodology allows one to design a control-charting tool to detect out-of-control deviations from the originating CAD model, translating the 3D shape-modelling problem into a 1D profile-monitoring framework. The real case study and the simulation analysis highlighted the fact that the proposed approach is effective in detecting even small local distortions that, though being hard to identify with the naked eye, may affect the mechanical performance of the structure. This approach is suitable in the presence of one-of-a-kind parts, as it allows identifying unit cells whose deviation from the nominal shape exhibits outlying patterns. Nevertheless, the methodology can be adapted to deal with series production applications, where copies of the same structure are manufactured. The presented analysis showed the potential of detecting local and global anomalies that may originate under out-of-control process conditions.

7.1 Future research and possible extensions of the proposed approach

In this study, we presented a quality monitoring method that could be applied to detect local anomalies in a structure consisting of unit cells of equal chape repeating in space and we showed the possible

extension of the method in the presence of a series production of copies of the same structure. The proposed approach relied on the assumption that the manufacturing process is stable with a cell-to-cell variability that is the same within all inspected parts. If different conditions apply, and they are compatible with the industrial needs, extensions of the proposed approach could be considered. One possible extension of the method can be considered in case the existence of a systematic location-dependent variation of cell properties within each structure is deemed acceptable as representative of the natural process signature. As an example, a possible variation of the monitored quantities may exist along one direction, e.g., the build direction, z. In this case, the monitoring statistics could be enriched by considering a hyper-modelling approach, where one monitoring statistic is associated to the parameters of the fitted 1-D deviation profile and another monitoring statistic is associated to the parameters of the $f(z)$ model describing the natural variation of deviation profile patterns in space.

Another extension of the proposed approach regards applications in which process optimization or process calibration is of interest. In that case, the modelling framework we are proposing, i.e., representing the cell evolution along Z as a deviation profile, could be used in the analysis of the effect of process parameters and process calibration procedures on the sources of variability. Indeed, different process parameters or different process settings may affect the cell evolution along the build direction: a methodology suitable to characterize such variation may aid the tuning of controllable factors to make the process more stable and repeatable.

Eventually, one great potential for the future industrial deployment of the proposed method consists in the possibility of using in-situ metrology, where the layer-wise geometry is identified by using in-situ machine vision tools (Grasso and Colosimo, 2017; Everton et al., 2016; Colosimo and Grasso, 2018), rather than ex-situ and post-process measurements. Indeed, additive manufacturing systems are more and more equipped with in-situ sensing systems that potentially enable the in-situ and in-line reconstruction of the printed shape on a layer-by-layer basis. The proposed method is based on a slice-by-slice comparison between the as-built and the as-designed geometry along the build direction. Thus, it could be possible to feed this method with layer-wise images gathered during the

production of the part in order to estimate the deviation directly in-line and in-situ. This is expected to yield a considerable reduction in post-process inspection costs and time together with an enhanced capability to anticipate the detection of geometrical distortions during the process itself.

Acknowledgements

References

Bui, A. T., & Apley, D. W. (2018). Monitoring for changes in the nature of stochastic textured surfaces. Journal of Quality Technology, 50(4), 363-378.

Callieri, M., Cignoni, P., Ganovelli, F., Montani, C., Pingi, P., & Scopigno, R. (2003, November). VCLab's Tools for 3D range data processing. In VAST (Vol. 3, pp. 5-7).

Chuang, S. C., Hung, Y. C., Tsai, W. C., & Yang, S. F. (2013). A framework for nonparametric profile monitoring. Computers & Industrial Engineering, 64(1), 482-491.

Colosimo, B. M., Cicorella, P., Pacella, M., & Blaco, M. (2014). From profile to surface monitoring: SPC for cylindrical surfaces via Gaussian processes. Journal of Quality Technology, 46(2), 95-113.

Colosimo, B. M. (2018). Modeling and Monitoring Methods for Spatial and Image Data. Quality Engineering, 30(1), 94-111.

Colosimo, B. M., Huang, Q., Dasgupta, T., & Tsung, F. (2018). Opportunities and challenges of quality engineering for additive manufacturing. Journal of Quality Technology, 50(3), 233-252.

Colosimo B.M., Grasso M. (2018). Spatially Weighted PCA for Monitoring Video Image Data with Application to Additive Manufacturing, Journal of Quality Technology, 50(4), 391-417.

Colosimo, B. M., Pacella, M., & Senin, N. (2015). Multisensor data fusion via Gaussian process models for dimensional and geometric verification. Precision Engineering, 40, 199-213.

Dallago, M., Raghavendra, S., Luchin, V., Zappini, G., Pasini, D., & Benedetti, M. (2019). Geometric assessment of lattice materials built via Selective Laser Melting. Materials Today: Proceedings, 7, 353-361.

Del Castillo, E., Colosimo, B. M., & Tajbakhsh, S. D. (2015). Geodesic Gaussian processes for the parametric

reconstruction of a free-form surface. Technometrics, 57(1), 87-99.

Del Castillo, E., & Zhao, X. (2019). Industrial statistics and manifold data. Quality Engineering, 1-13.

Everton, S. K., Hirsch, M., Stravroulakis, P., Leach, R. K., & Clare, A. T. (2016). Review of in-situ process monitoring and in-situ metrology for metal additive manufacturing. Materials & Design, 95, 431-445.

Galjaard, S., Hofman, S., Ren, S., (2014) Advances in Architectural Geometry, Arup, Amsterdam, The Netherlands © Springer International Publishing Switzerland, P. Block et al. (eds.), 79-93

Gardner, M.M., Lu, J-C., Gyurcsik, R.S. (1997). Equipment Fault Detection Using Spatial Signatures, IEEE Transactions on Components, Packaging, and Manufacturing Technology-Part C, 20(4), 295-304

Goldenthal, R. and Bercovier, M. (2004). "Spline Curve Approximation and Design by Optimal Control Over the Knots". Computing 72(1–2), pp. 53–64.

Gomaa, A. S., & Birch, J. B. (2019). A semiparametric nonlinear mixed model approach to phase I profile monitoring. Communications in Statistics-Simulation and Computation, 48(6), 1677-1693.

Grasso M., Colosimo B.M., (2017), Process Defects and In-situ Monitoring Methods in Metal Powder Bed Fusion: a Review, Measurement Science and Technology, 28(4), 1-25, DOI: 10.1088/1361-6501/aa5c4f

Grasso M., Menafoglio A., Colosimo B. M., Secchi P. (2016), Using Curve Registration Information to Enhance Profile Monitoring of Signal Data, Journal of Quality Technology, 48(2), 99-127

Hadidoust, Z., Samimi, Y., & Shahriari, H. (2015). Monitoring and change-point estimation for spline-modeled non-linear profiles in phase II. Journal of Applied Statistics, 42(12), 2520-2530.

Han, C., Li, Y., Wang, Q., Wen, S., Wei, Q., Yan, C., ... & Shi, Y. (2018). Continuous functionally graded porous titanium scaffolds manufactured by selective laser melting for bone implants. Journal of the mechanical behavior of biomedical materials, 80, 119-127.

Hanks, B., Berthel, J., Frecker, M., & Simpson, T. W. (2020). Mechanical properties of additively manufactured metal lattice structures: data review and design interface. Additive Manufacturing, 35, 101301.

He, L., Grasso, M., Colosimo, B.M., Huang, Q., (2019), Prescriptive Data-Analytical Modeling of Laser Powder Bed Fusion Processes, Journal of Manufacturing Science and Technology, doi:10.1115/1.4041709

He, K., Zhang, M., Zuo, L., Alhwiti, T., and Megahed, F. (2017). Enhancing the monitoring of 3D scanned manufactured parts through projections and spatiotemporal control charts. Journal of Intelligent Manufacturing, 28:899–911.

Holz, D., Ichim, A. E., Tombari, F., Rusu, R. B., & Behnke, S. (2015). Registration with the point cloud library: A modular framework for aligning in 3-D. IEEE Robotics & Automation Magazine, 22(4), 110-124.

Huang, D., Du, S., Li, G., Zhao, C., & Deng, Y. (2018). Detection and monitoring of defects on three-dimensional

curved surfaces based on high-density point cloud data. Precision Engineering, 53, 79-95.

Komarek, M. (2017). Design of spacecraft components for Additive manufacturing, L.K.Engineering, https://www.lke.cz/mt-content/uploads/2017/11/design-of-spacecraft-components-for-additive-manufacturing.pdf

ISO/ASTM (2019). Additive Manufacturing – Process Characteristics and Performance: Practice for Metal Powder Bed Fusion Process to Meet Critical Applications, ISO/ASTM 52904:2019(E)

Lee, H. Y., and D. W. Apley. 2004. Diagnosing manufacturing variation using second-order and fourth-order statistics. International Journal of Flexible Manufacturing, Systems 16:45–64.

Lin, H. D., and S. W. Chiu. 2006. Computer-aided vision system for MURA-type defect inspection in liquid crystal displays. Paper presented at the Pacific-Rim Symposium on Image and Video Technology, Hsinchu, Taiwan, December 10-13.

Lin, H. D. 2007a. Automated visual inspection of ripple defects using wavelet characteristic based multivariate statistical approach. Image and Vision Computing 25 (11):1785–801. doi:10.1016/j.imavis.2007.02.002

Lin, H. D. 2007b. Computer-aided visual inspection of surface defects in ceramic capacitor chips. Journal of Materials Processing Technology 189 (1–3):19–25. doi:10.1016/j.jmatprotec.2006.12.051

Lin, H. D., C. Y. Chung, and W. T. Lin. 2008. Principal component analysis based on wavelet characteristics applied to automated surface defect inspection. WSEAS Transactions on Computer Research 3 (4):193–202.

Liu, L., Kamm, P., García-Moreno, F., Banhart, J., & Pasini, D. (2017). Elastic and failure response of imperfect three-dimensional metallic lattices: the role of geometric defects induced by Selective Laser Melting. Journal of the Mechanics and Physics of Solids, 107, 160-184.

Megahed, F. M., W. H. Woodall, and J. A. Camelio. (2011). A review and perspective on control charting with image data. Journal of Quality Technology 43 (2):83–98. doi: 10.1080/00224065.2011.11917848

Megahed, F., Wells, L., & Camelio, J. (2010). The use of 3D laser scanners in statistical process control (No. 2010-01-1864). SAE Technical Paper.

Melancon, D., Bagheri, Z. S., Johnston, R. B., Liu, L., Tanzer, M., & Pasini, D. (2017). Mechanical characterization of structurally porous biomaterials built via additive manufacturing: experiments, predictive models, and design maps for load-bearing bone replacement implants. Acta biomaterialia, 63, 350-368.

Menafoglio, A., Grasso, M., Secchi, P., & Colosimo, B. M. (2018). Profile monitoring of probability density functions via simplicial functional PCA with application to image data. Technometrics, 60(4), 497-510.

Molinari, N.; Durand, J. F.; and Sabatier, R. (2004). "Bounded Optimal Knots for Regression Splines". Computational Statistics & Data Analysis 45(2), pp. 159–178.

Montgomery, D. C. (2008), Introduction to Statistical Quality Control (6th ed.), New York: Wiley.

NASA (2017a). Specification For Control And Qualification Of Laser Powder Bed Fusion Metallurgical Processes, MSFC-SPEC-3717, October 18, 2017

NASA (2017b). Standard For Additively Manufactured Spaceflight Hardware By Laser Powder Bed Fusion In Metals, MSFC-SPEC-3716, October 18, 2017

Pulli, K. (1999). Multiview registration for large data sets. In *Second International Conference on 3-D Digital Imaging and Modeling (Cat. No. PR00062)* (pp. 160-168). IEEE.

Ramsay, J. O. (2004). Functional data analysis. Encyclopedia of Statistical Sciences, 4.

Rusinkiewicz, S., & Levoy, M. (2001). Efficient variants of the ICP algorithm. In 3dim (Vol. 1, pp. 145-152).

Sangalli, L. M.; Secchi, P.; Vantini, S.; and Veneziani, A. (2009). "Efficient Estimation of Three-Dimensional Curves and Their Derivatives by Free-Knot Regression Splines, Applied to the Analysis of Inner Carotid Artery Centrelines". Journal of the Royal Statistical Society, Series C (Applied Statistics) 58(3), pp. 285–306.

Senin, N., Colosimo, B. M., & Pacella, M. (2013). Point set augmentation through fitting for enhanced ICP registration of point clouds in multisensor coordinate metrology. Robotics and Computer-Integrated Manufacturing, 29(1), 39-52.

Shan, X., and D. W. Apley. 2008. Blind identification of manufacturing variation patterns by combining source separation criteria. Technometrics 50:332–343.

Shi, Z., Apley, D. W., & Runger, G. C. (2019). Identifying and visualizing part-to-part variation with spatially dense optical dimensional metrology data. Journal of Quality Technology, 51(1), 3-20.

Stankus, S. and Castillo-Villar, K. (2018). An improved multivariate generalised likelihood ratio control chart for the monitoring of point clouds from 3D laser scanners. International Journal of Production Research, 57:1–12.

Tsung, F., Zhang, K., Cheng, L., & Song, Z. (2018). Statistical transfer learning: A review and some extensions to statistical process control. Quality Engineering, 30(1), 115-128.

Van Bael, S., Kerckhofs, G., Moesen, M., Pyka, G., Schrooten, J., & Kruth, J. P. (2011). Micro-CT-based improvement of geometrical and mechanical controllability of selective laser melted Ti6Al4V porous structures. Materials Science and Engineering: A, 528(24), 7423-7431.

Wang, A., Wang, K., & Tsung, F. (2014). Statistical surface monitoring by spatial-structure modeling. Journal of Quality Technology, 46(4), 359-376.

Wang, Y., Arabnejad, S., Tanzer, M., & Pasini, D. (2018). Hip implant design with three-dimensional porous architecture of optimized graded density. Journal of Mechanical Design, 140(11).

Wells, L. J., Megahed, F. M., Niziolek, C. B., Camelio, J. A., and Woodall, W. H. (2013). Statistical process monitoring

approach for high-density point clouds. Journal of Intelligent Manufacturing, 24(6):1267–1279.

Williams, J. D., Woodall, W. H., & Birch, J. B. (2007). Statistical monitoring of nonlinear product and process quality profiles. Quality and Reliability Engineering International, 23(8), 925-941.

Woodall, W. H. (2007). Current research on profile monitoring. Production, 17(3), 420-425.

Wu, X., Su, Y., & Shi, J. (2019). Perspective of additive manufacturing for metamaterials development. Smart Materials and Structures, 28(9), 093001.

Zang, Y., & Qiu, P. (2018a). Phase I monitoring of spatial surface data from 3D printing. Technometrics, 60(2), 169-180.

Zang, Y., & Qiu, P. (2018b). Phase II monitoring of free-form surfaces: An application to 3D printing. Journal of Quality Technology, 50(4), 379-390.

Zhao, X., and E. del Castillo. 2019. An intrinsic geometrical approach for statistical process control of surface and manifold data. arXiv preprint arXiv:1907.00111.

Zhou, S. and Shen, X. (2001). "Spatially Adaptive Regression Splines and Accurate Knot Selection Schemes". Journal of the American Statistical Association 96(453), pp. 247–259.